

Analytical invariant manifolds near unstable points and the structure of chaos

C. Efthymiopoulos, G. Contopoulos, and M. Katsanikas

Research Center for Astronomy and Applied Mathematics
Academy of Athens, Soranou Efessiou 4, 115 27 Athens, Greece

Keywords: Hyperbolic normal form; Invariant manifolds; Homoclinic chaos

Abstract: It is known that the asymptotic invariant manifolds around an unstable periodic orbit in conservative systems can be represented by convergent series (Cherry 1926, Moser 1956, 1958, Giorgilli 2001). The unstable and stable manifolds intersect at an infinity of homoclinic points, generating a complicated homoclinic tangle. In the case of simple mappings it was found (Da Silva Ritter et al. 1987) that the domain of convergence of the formal series extends to infinity along the invariant manifolds. This allows in practice to study the homoclinic tangle using only series. However in the case of Hamiltonian systems, or mappings with a finite analyticity domain, the convergence of the series along the asymptotic manifolds is also finite. Here, we provide numerical indications that the convergence does not reach any homoclinic points. We discuss in detail the convergence problem in various cases and we find the degree of approximation of the analytical invariant manifolds to the real (numerical) manifolds as i) the order of truncation of the series increases, and ii) we use higher numerical precision in computing the coefficients of the series. Then we introduce a new method of series composition, by using action-angle variables, that allows the calculation of the asymptotic manifolds up to an arbitrarily large extent. This is the first case of an analytic development that allows the computation of the invariant manifolds and their intersections in a Hamiltonian system for an extent long enough to allow the study of homoclinic chaos by analytical means.

1 Introduction

It is well known that the formal series representing the invariant manifolds (tori) near stable equilibria or stable periodic orbits in Hamiltonian systems are not convergent in general (for a review see Contopoulos 2002), except in the case of integrable systems. However, near unstable equilibria, or unstable periodic orbits, the invariant manifolds can be represented by *convergent* formal series (Cherry 1926, Moser 1956, 1958) (see also Bruno 1971, 1989, Giorgilli 2001, Delshams and Lázaro 2005).

The motion near the unstable points takes place along such invariant manifolds. On the other hand, near these points there is chaos. Thus the question is how is it possible for convergent (analytic) series to represent chaotic motions.

The structure of chaos near the unstable points is determined by the intricate forms of the stable and unstable asymptotic manifolds, which intersect in a complicated way forming the so-called homoclinic or heteroclinic tangles. So far, these structures have been studied in concrete examples mainly by numerical means (e.g. Bertlett 1978, Bartlett 1982, Bartlett 1989, Contopoulos 1990, Roeder et al. 2003, Contopoulos and Polymilis 1993, Bazzani et al. 1993, Contopoulos et al. 1994, Contopoulos et al. 1996, Rom-Kedar 1990, Evans et al. 2004, Polymilis et al. 2003). For computations related to celestial mechanics see Simo 1990, Jorba and Masdemont 1999, Perozzi and Ferraz-Mello 2010, Gómez and Barradés 2011 and

references therein.

Nevertheless, little has been done *analytically* to explore the convergent series expansions in order to study the chaotic structures formed by the invariant manifolds. This was due to the fact that the domain of convergence established in the original theorems of Moser is finite, and in general it is considered to be rather small.

However, the question of the true size of the domain of convergence is still open. In an early calculation, Franceschini and Russo (Franceschini and Russo 1981) computed several lobes and homoclinic points of the asymptotic manifolds in the 2D Hénon mapping using a variant of the normal form series approach. In a more general context, Da Silva Ritter et al. (Da Silva Ritter et al. 1987) have shown that in the case of some simple 2D symplectic mappings analytic and with an analytic inverse over the whole plane, the domain of convergence along the asymptotic invariant manifolds extends to *infinity*. (As pointed out in the historical notes of Cabré et al. (2005), this property is a direct consequence of a theorem of functional analysis going back to Poincaré (Poincaré 1890)). This property allows to reproduce many non-trivial features of the homoclinic tangle using only series.

On the other hand, it was up to now unknown whether a similar extension applies in the case of Hamiltonian flows as well (see Vieira and Ozorio de Almeida 1996, Ozorio de Almeida and Vieira 1997).

In the present paper we make a detailed numerical study of the size of the domain of convergence of the hyperbolic normal form series both in 2D mappings and in 2D Hamiltonian systems. In particular, we perform an analytical computation of the invariant manifolds up to high truncation orders, and provide evidence regarding i) how well they can represent the true form of the invariant manifolds, and ii) what is the extent of the domain of convergence.

Regarding this last question, we note, first, the well known fact that the non-convergence or convergence of the formal series is related to the appearance or non-appearance, in the series, of *small divisors*. In the case of systems of two degrees of freedom, near a stable periodic orbit we have in general divisors of the form $m_1\omega_1 + m_2\omega_2$, with m_1, m_2 integer and ω_1, ω_2 real. Such divisors can become very small when $|m| = |m_1| + |m_2|$ becomes large, or zero when ω_1, ω_2 are commensurable. The latter (resonant) case requires a special treatment, which, however, presents similar non-convergence features as the non-resonant case. On the other hand, in the case of unstable periodic orbits we have two frequencies ω_1 (real) and $\omega_2 = -i\nu$ (imaginary). Then, it can be shown that the corresponding divisors never approach very close to zero, since they are bounded by a quantity $|m|\gamma$, where γ is a positive constant of the order of the minimum of $|\omega_1|$ or $|\nu|$ (see Giorgilli 2001).

The first proof of the convergence of the formal series was provided by Cherry (1926), while a more general proof was provided by Moser (1956, 1958) and Giorgilli (2001). The first paper of Moser (1956) refers to 2D area preserving maps. In this case, the unstable fixed points correspond to unstable periodic orbits on the surface of section of two degrees of freedom Hamiltonian systems. On the other hand, the second paper (Moser 1958) investigates N-degree of freedom Hamiltonian systems of the form $H(x, y) = H_0(x, y) + H_1(x, y) + \dots$, where $x \equiv (x_1, \dots, x_N)$, $y \equiv (y_1, \dots, y_N)$, are canonical positions and momenta, and H_i are polynomials in (x, y) of degree $i + 2$, with a quadratic part

$$H_0 = \sum_{j=1}^N i\omega_j x_j y_j \quad (1)$$

with ω_1/ω_2 non-real, and $k_1\omega_1 + k_2\omega_2 \neq \omega_j$ for all integers k_1, k_2 and all $j > 2$. The case of unstable equilibrium in two degrees of freedom systems corresponds to ω_1 real, and $\omega_2 = -i\nu$ imaginary, while, for more than two degrees of freedom, the theorem applies also to complex

unstable points (i.e. ω_1, ω_2 complex). Moser's theorem then establishes the existence of special solutions of the Hamiltonian equations of motion in which all variables x_j, y_j can be expressed via four parameters (q, p, ξ, η) , i.e. of the form $x_j = X_j(q, p, \xi, \eta)$, $y_j = Y_j(q, p, \xi, \eta)$, such that for the variables (q, p, ξ, η) we have the 'normal form' time evolution given by

$$q = q_0 e^{i\Omega(J,c)t}, \quad p = p_0 e^{-i\Omega(J,c)t}, \quad \xi = \xi_0 e^{\Lambda(J,c)t}, \quad \eta = \eta_0 e^{-\Lambda(J,c)t} \quad (2)$$

with $\Omega = \omega_1 + \dots$, $\Lambda = \nu + \dots$, and $J = iq_0 p_0$, $c = \xi\eta$. The quantities J, c represent integrals of motion of Moser's normal form, since we have $\dot{q}(t)p(t) = -iJ$, $\dot{\xi}(t)\eta(t) = c$ for all times t . In particular: i) the values $c = J = 0$ correspond to the unstable equilibrium point, and ii) the values $J \neq 0, c = 0$ correspond to unstable periodic orbits with a frequency equal to $\Omega(J, 0)$, as well as to their *asymptotic orbits* lying on the invariant manifolds of the periodic orbits. Finally, iii) the values $c \neq 0$ correspond to orbits in the neighborhood of the unstable periodic orbits (or points), subject to locally hyperbolic dynamics under the Eqs.(2).

The theorem of Moser was completed in an essential way by Giorgilli (2001), who demonstrated that the special solutions of Moser can be recovered via a convergent *canonical* transformation of the variables (x, y) , such that in the new canonical variables the Hamiltonian resumes a normal form leading to the solutions (2). In the theorem of Giorgilli, one still has no small divisors, and the proof of the convergence of the normalizing transformation in a domain surrounding the origin follows by a proper control of the Cauchy estimates (see Giorgilli 2002 for a review) applying to the derivatives of various analytic functions appearing in the normalization canonical procedure. For a discussion of the convergence properties of the hyperbolic normal form series nonlinear flows see also Bruno (1971), Delshams and Lázaro (2005).

The theorems of Moser and Giorgilli guarantee the existence of a disc of finite radius of convergence of the hyperbolic normal form series around the origin. However, the true extent as well as the true shape of the domain of convergence are not yet fully understood. Da Silva Ritter et al. (1987) demonstrated that in the case of simple conservative 2D mappings (i.e. mappings represented by analytic functions over the whole phase space) the domain of convergence of the hyperbolic normal form series goes to infinity along the axes $\xi = 0$ and $\eta = 0$ of the new canonical variables resulting after the mapping's normalizing transformation. Since these axes represent the stable and the unstable manifolds of the unstable point, this property permits in practice a purely analytic computation of the invariant manifolds and of all features connected with homoclinic dynamics, using only series (and not numerical integration methods).

In order to verify this fact, we presently compute the hyperbolic normal form in two simple 2D symplectic mappings, namely the standard map and the Hénon map. In order to estimate the radius of absolute convergence of the hyperbolic series along particular directions from the origin, we use D'Alembert's criterion. We then find that the successive radii ρ_r of the D'Alembert sequence yield larger and larger values as the truncation order r increases, thus providing evidence that the successive values ρ_r tend to infinity as $r \rightarrow \infty$. Furthermore, we find that the rate of increase of ρ_r with r is different in the case of the standard map than in the case of the Hénon map. Namely, we have a logarithmic dependence $\rho_r \sim \log(r)$ in the former, while we find a power-law dependence $\rho_r \sim r^p$, with $p \simeq 2$, in the latter. Nevertheless, when back-transforming to the original variables, in both maps we find that the series truncated at order r represent successfully the invariant manifolds up to an extent whose length scales as $\sim \log(r)$.

On the other hand, in Hamiltonian systems of two degrees of freedom, some numerical calculations (see, for example, Fig.4 of Vieira and Ozorio de Almeida (1996), and Fig.2 of

Bongini et al. (2001)) give the impression that the domain of convergence of Moser’s normal form should extend at most up to the point where the two branches $\xi = 0$ and $\eta = 0$ (stable and unstable manifolds) of the invariant curve $\xi\eta = c = 0$, when transformed to curves in the original canonical variables, intersect each other at a homoclinic point. According to Bongini et al. (2001), such a point constitutes a “singularity” of the formal expansions that “defines the applicability limit of the normal form dynamics”.

Despite these indications, Vieira and Ozorio de Almeida (1996) have conjectured that the domain of convergence of Moser’s normal form may extend long enough as to include homoclinic points. In fact, the same authors presented numerical calculations by which it was apparently possible to compute a homoclinic intersection in the Hénon-Heiles 2D Hamiltonian model which possesses a (triple) hyperbolic equilibrium point. However, a careful examination of their calculations reveals that the computation was partly based on numerical propagation of the orbits and not exclusively on series. On the other hand, a purely analytic computation, based on series up to the 16th degree, failed to give a precise location of even one homoclinic point.

In Ozorio de Almeida and Vieira (1997), the authors invoke an argument according to which, using repeatedly *analytic continuation* (see our section 4), it becomes possible to obtain the time evolution of all initial conditions at $t = 0$ along the Hamiltonian flow under the form of a symplectic mapping connecting the initial conditions with the values of the canonical variables at a later time t . As we shall see, however, the fact that this mapping has a limited domain of analyticity introduces a crucial difference between the Hamiltonian and the simple mapping cases, thus, not allowing for the extension of the domain of convergence proposed by Ozorio de Almeida and Vieira to apply in the case of Hamiltonian flows.

Our own main results in the present paper regarding the Hamiltonian case can be summarized as follows:

1) We compute the hyperbolic series around unstable periodic orbits in generic Hamiltonian systems expressed in action - angle variables, of which the polynomial Hamiltonian systems with unstable equilibria considered by Moser are a special case. In such systems, we provide strong numerical indications that the domain of convergence of the hyperbolic series is finite, and that it contains no homoclinic intersections.

2) However, we propose a new method, which materializes the main idea of the analytic continuation technique of Ozorio de Almeida and Vieira (1997), and allows to obtain a parametrization of the invariant manifolds using only series in a domain extending well beyond the limit of convergence of the original series. This, in turn, allows to compute many homoclinic intersections and the lobes formed by the invariant manifolds using only series.

3) In the case of systems of non-polynomial form that can be written in action-angle variables, the main element of our method is to use truncated Fourier series *not expanded in the angles* around the unstable point. In fact, we exploit the property of the Fourier series that their singularity with respect to the angles is on the imaginary axis, while all computations with the angles lying on the real axis remain convergent.

4) We show that the accuracy of computations depends (a) on the order of truncation of the series, and (b) on the number of digits used in calculating the coefficients of the series.

5) Furthermore, we define ‘invariant’ and ‘quasi-invariant’ curves on the surface of section corresponding to values of $c \neq 0$. For small values of c they correspond to initial conditions that are mapped onto segments of the same curve up to an extent large enough to include several oscillations and lobes similar to those of the asymptotic manifolds (see detailed definitions in section 4). Thus, such curves characterize the structure of chaos in the neighborhood of the unstable periodic orbit. Also, they have self-intersections, which, as shown in Da Silva

Ritter et al. (1987) can be exploited in order to compute high order periodic orbits accumulating to one or more homoclinic points. Our analytical method facilitates the computation of such orbits. However, a detailed study of such computations is deferred to a future work.

The paper is organized as follows. In section 2 we present our results for the convergence of the hyperbolic normal form series and the analytic computation of invariant manifolds in 2D symplectic mappings. Section 3 presents our Hamiltonian model as well as the algorithm of computation of the hyperbolic normal form series in the Hamiltonian case. We also find analytically the characteristic curve, i.e., the position of the basic unstable periodic orbit as a function of our model's perturbation parameter ϵ . Then, we study numerically the domain of convergence in the Hamiltonian model. In section 4 we introduce our extended analytical method of computation of the invariant manifolds, and demonstrate its use in the computation of the structure of the homoclinic tangle and its neighborhood. In section 5 we study the convergence properties of the hyperbolic normal form as well as the application of our extended method in a polynomial Hamiltonian system which reduces to the case considered by Moser exactly. Section 6 is a summary of our basic conclusions.

2 Analytical invariant manifolds in symplectic mappings: convergence

In order to emphasize the difference between the Hamiltonian and the mapping cases, we will consider first the computation of the invariant manifolds and the convergence of the hyperbolic normal form in the case of 2D symplectic mappings. It should be noted that such mappings have recently found use in the study of manifold dynamics in problems of astrodynamics (e.g. Ross and Scheeres 2007, Grover and Ross 2009, Campagnola et al. 2012). Nevertheless, as shown below, the domain of applicability of analytical computations of invariant manifolds in such cases depends crucially on the extent of the domain of analyticity of the original mapping.

We consider real-analytic 2D symplectic mappings $M : (u_1, u_2) \rightarrow (u'_1, u'_2)$ of the form:

$$\begin{aligned} u'_1 &= \lambda_1 u_1 + F_2(u_1, u_2) + F_3(u_1, u_2) + \dots \\ u'_2 &= \lambda_2 u_2 + G_2(u_1, u_2) + G_3(u_1, u_2) + \dots \end{aligned} \quad (3)$$

where $\lambda_1 = e^\nu$, $\lambda_2 = \frac{1}{\lambda_1} = e^{-\nu}$, with $\nu > 0$, and F_s, G_s are polynomials of degree s in the variables (u_1, u_2) . A mapping of the form (3) possesses an unstable fixed point at the origin $(0, 0)$. In order to compute its manifolds, we look for a near-identity canonical transformation $\Phi \equiv (\Phi_1, \Phi_2)$ defined by

$$\begin{aligned} u_1 &= \Phi_1(\xi, \eta) = \xi + \Phi_{1,2}(\xi, \eta) + \Phi_{1,3}(\xi, \eta) + \dots \\ u_2 &= \Phi_2(\xi, \eta) = \eta + \Phi_{2,2}(\xi, \eta) + \Phi_{2,3}(\xi, \eta) + \dots \end{aligned} \quad (4)$$

where $\Phi_{i,s}$ are polynomials of degree s in the new canonical variables (ξ, η) , so that the mapping (3) expressed in the variables (ξ, η) takes the normal form

$$\begin{aligned} \xi' &= W_1(\xi, \eta) = \Lambda(c)\xi = (\lambda_1 + w_2 c + w_3 c^2 + \dots)\xi \\ \eta' &= W_2(\xi, \eta) = (1/\Lambda(c))\eta = (\lambda_2 + v_2 c + v_3 c^2 + \dots)\eta \end{aligned} \quad (5)$$

where $c = \xi\eta$, and w_s, v_s are real constants. The unstable and stable manifolds correspond to the value $c = 0$, and they coincide with the axes $\eta = 0$ (unstable manifold) or $\xi = 0$

(stable manifold). Back-transforming to the original variables yields the form of the invariant manifolds as functions of the co-ordinate parameters ξ and η respectively.

The details of how to compute the transformation Φ are given in da Silva Ritter et al. (1987) (in fact, they are not different from the classical computation of the Birkhoff normal form for 2D mappings with an equilibrium point at the origin).

We implemented the above procedure in the case of the unstable point $(0,0)$ of the standard map

$$\begin{aligned}x'_1 &= x_1 + K \sin(x_1 + x_2) \\x'_2 &= x_1 + x_2\end{aligned}\tag{6}$$

for $K = 1.3$, and of the Hénon map

$$\begin{aligned}x'_1 &= \cosh(a)x_1 + \sinh(a)x_2 - \frac{\sqrt{2}}{2} \sinh(a)x_1^2 \\x'_2 &= \sinh(a)x_1 + \cosh(a)x_2 - \frac{\sqrt{2}}{2} \cosh(a)x_1^2\end{aligned}\tag{7}$$

for $a = 1.43$ (as in Da Silva Ritter et al. 1987). The mappings (6) and (7) resume the form (3) after a linear symplectic diagonalizing transformation.

Figures 1a,b,c,d show a comparison between numerical and analytical invariant manifolds computed by the above method, using the series up to the truncation orders $r = 20$ (Fig.1a,c), and $r = 60$ (Fig.1b,d). We note immediately that the analytical manifolds fit very well the numerical ones up to several homoclinic intersections, whose number increases with r . Also, the analytical manifolds reproduce the oscillations and the lobes characteristic of the homoclinic dynamics to an extent also increasing with r .

In the case of both the above mappings, the form (3) represents a function analytic over the *whole* plane (u_1, u_2) . When this property holds true, Da Silva Ritter et al.(1987) proved that the domain of convergence of the normalizing transformation Φ should extend to infinity along the axes $\xi = 0$ and $\eta = 0$. In fact, we can probe numerically the convergence of Φ along the axes $\xi = 0$ and $\eta = 0$ using *D'Alembert's criterion*. Namely, if we set $\eta = 0$ in the normalizing transformation Φ , we find expressions of the form

$$u_1 = \xi + g_2\xi^2 + g_3\xi^3 + \dots, \quad u_2 = g'_2\xi^2 + g'_3\xi^3 + \dots\tag{8}$$

The D'Alembert sequence of radii is defined by

$$\rho_r = \left| \frac{g_{r-1}}{g_r} \right|, \quad r = 2, 3, \dots\tag{9}$$

The limit $\lim_{r \rightarrow \infty} \rho_r$ yields the radius of absolute convergence along the axis $\eta = 0$ (unstable manifold). Figure 2 shows ρ_r versus r for the truncation orders $r = 2, 3, \dots, 60$ in both mappings. We have a clear indication that ρ_r goes to infinity in both cases. However, a clear difference is that in the case of the standard map (Fig.2a) the increase of ρ_r with r seems to be logarithmic ($\rho_r \sim \log(r)$), while in the case of the Hénon map (Fig.2b) it seems to be close to quadratic $\rho_r \sim r^2$. Nevertheless, even in the latter case, when we compute the length of the invariant manifolds in the *original* canonical variables up to the point $(\xi = \rho_r, \eta = 0)$ (for the unstable manifold), we find that the length increases always logarithmically with r . This property sets a practical limit to the extent of the manifolds that can be computed analytically. At any rate, the most important remark is that even this limit is influenced by

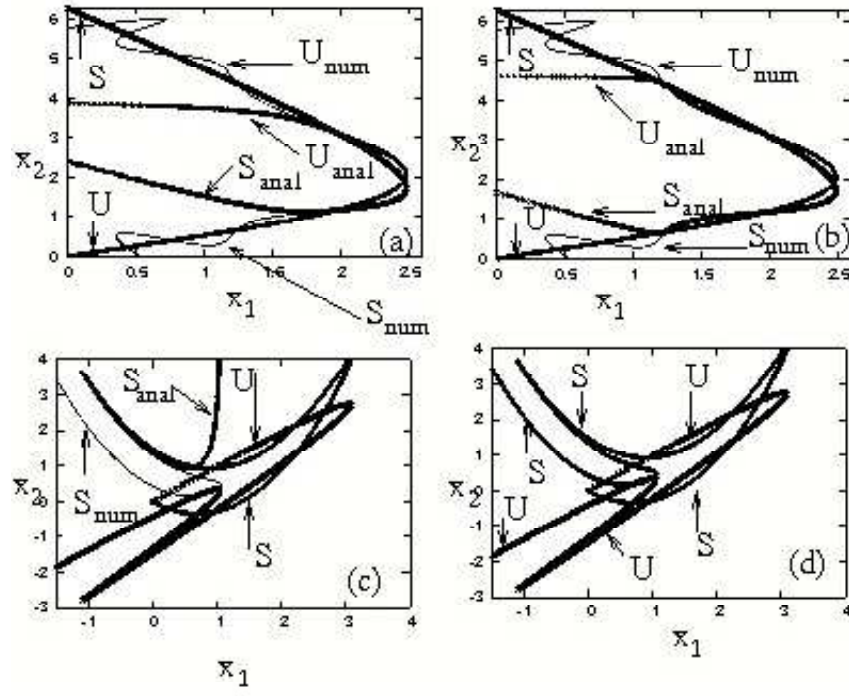


Figure 1: Numerical (thin line) and analytical calculation (thick line) of the invariant manifolds in the case of the standard map at orders (a) 20 and (b) 60, and in the case of the

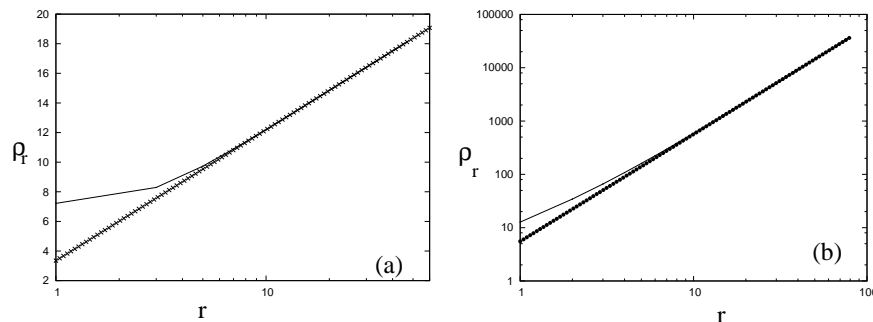


Figure 2: The sequence of D'Alembert radii found by the coefficients of the normalizing transformation Φ_1 for $\eta = 0$ (see text), versus the normalization order r for (a) the standard map, and (b) the Hénon map. In (a) we find the fitting law $\rho_r = 3.34966 + 3.83952 \log(r)$. In (b), we find a power fitting law $\rho_r = 5.52r^{2.01}$ (thick lines).

the extent of the domain of analyticity of the original mapping. Thus, for example, if instead of the standard mapping we use a variant of the form

$$\begin{aligned} x'_1 &= x_1 + \frac{K \sin(x_1 + x_2)}{2 - \cos(x_1 + x_2)} \\ x'_2 &= x_1 + x_2 \quad . \end{aligned} \tag{10}$$

which possesses the same unstable point at the origin, with precisely the same eigenvalues and eigenvectors as the standard map (6), we find that the analytical computation of the invariant manifolds in that case diverges beyond a domain that does not include any homoclinic point. This is due to the fact that the mapping (10) has a finite domain of analyticity $|x_1 + x_2| < 1.31696$. Thus, the analytical computation of the invariant manifolds cannot go beyond this domain. Note that singularities of the form of the map (10) are typical in applications of astrodynamics, where the domain of analyticity cannot extend beyond the distance of the considered unstable equilibrium point from any one of the bodies.

We will then pass to our main question, i.e. how do the above results compare with the extent of the domain of convergence of the hyperbolic normal form series in the Hamiltonian case.

3 Analytic manifolds in a Hamiltonian model

3.1 The model

We consider first a Hamiltonian system of one and a half degrees of freedom corresponding to a periodically driven pendulum model with explicit dependence on time. The Hamiltonian is

$$H = \frac{p^2}{2} - \omega_0^2(1 + \epsilon(1 + p) \cos \omega t) \cos \psi \quad . \tag{11}$$

Introducing a dummy action I , and its conjugate angle $\phi = \omega t$, with $\omega = 1$, the Hamiltonian can be written equivalently as

$$H(\psi, \phi, p, I) = \frac{p^2}{2} + \omega I - \omega_0^2(1 + \epsilon(1 + p) \cos \phi) \cos \psi \quad . \tag{12}$$

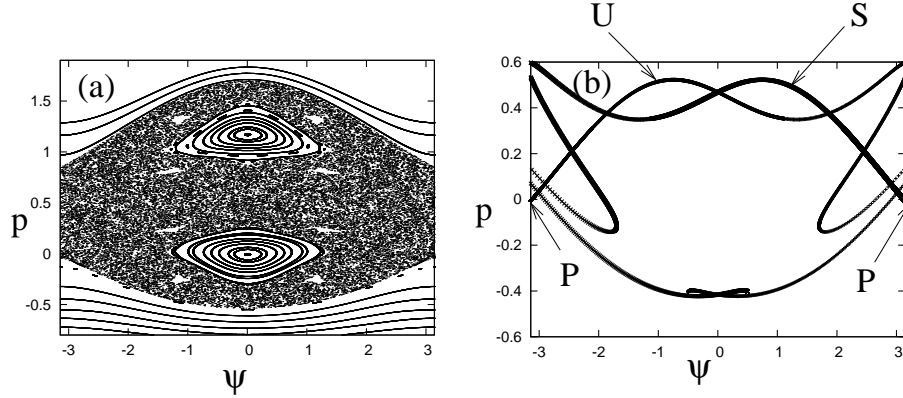


Figure 3: (a) The phase portrait (stroboscopic surface of section $(\psi(nT), p(nT))$) for the Hamiltonian system (12) for $\epsilon = 1$, $\omega_0 = 0.2\sqrt{2}$ and $\omega = 1$. (b) The form of the stable (W_S) and unstable W_U manifolds of the main unstable periodic orbit P , given modulo 2π at the above parameter values.

Figure 3a shows the phase portrait for $\epsilon = 1$, when $\omega_0 = 0.2\sqrt{2}$, $\omega = 1$. The phase portrait is obtained by a stroboscopic plot of all points $(\psi(nT), p(nT))$ along particular orbits at the successive times $t = nT$, $n = 1, 2, \dots$, where $T = 2\pi/\omega$ is the perturber's period. We observe that in the libration domain and in a large domain above it (with $p > 0$) most trajectories are chaotic. We distinguish only a large island in the libration domain, as well as one conspicuous 1:1 resonant island and some other smaller islands hosting quasi-periodic trajectories. Above and below the chaotic domain, we have many rotational invariant KAM curves.

The principal domain of chaos is caused by the homoclinic tangle of the invariant manifolds of a main unstable periodic orbit (denoted hereafter as P) of the Hamiltonian (12), which is formed as the continuation of the unstable equilibrium point at $\psi = \pi$ (or $-\pi$), $p = 0$ of the pendulum case ($\epsilon = 0$). For $\epsilon \neq 0$, this periodic orbit yields a fixed point $\psi_0 = \pm\pi$, $p_0(\epsilon) < 0$ on the stroboscopic surface of section $(\psi(nT), p(nT))$. For $\epsilon = 1$, we have $p_0 = -7.32464987 \times 10^{-3}$.

The intersection of the invariant manifolds of P with the surface of section $(\psi(nT), p(nT))$ is shown in Fig.3b. This is a purely numerical computation of the manifolds, obtained by iterating an initial segment of length $DS = 10^{-4}$ along the unstable or the stable eigendirections, in the forward or backward sense of time respectively. Due to the particular form of the Hamiltonian (11), the manifolds, as in fact the whole chaotic domain, have well developed lobes in the upper part of the chaotic layer (for $p > 0$), but not so much in the lower part which is delimited by the presence of rotational KAM curves.

3.2 Hyperbolic normal form

In order to compute a hyperbolic normal form for the Hamiltonian (12), we first Taylor-expand the Hamiltonian (12) in the neighborhood of the point $\psi_0 = \pi$ (or, equivalently, $-\pi$). Setting $\psi = \pi + u$, up to fourth order we have

$$H = \frac{p^2}{2} + \omega I - 0.08 \left(1 + 0.5\epsilon(1+p)(e^{i\phi} + e^{-i\phi}) \right) \left(-1 + \frac{u^2}{2} - \frac{u^4}{24} - \dots \right). \quad (13)$$

From this development we see that u (and ψ) corresponds to the hyperbolic degree of freedom, while ϕ corresponds to the elliptic degree of freedom. The difference between the two angles

appearing in the hyperbolic and elliptic degrees of freedom is crucial in the discussion of section 4 below. The hyperbolic part of the Hamiltonian has the form $H_h = p^2/2 - \nu^2 u^2/2$ where $\nu^2 = 0.08$. We then introduce the linear canonical transformation:

$$p = \frac{\sqrt{\nu}(\xi + \eta)}{\sqrt{2}}, \quad u = \frac{(\xi - \eta)}{\sqrt{2\nu}} \quad (14)$$

where ξ and η are the new canonical position and momentum respectively. Then H_h acquires the form $H_h = \nu\xi\eta$.

For the computation of the hyperbolic normal form, we introduce a variant of the algorithm proposed by Giorgilli (2001). The main change is that for the oscillatory degree of freedom we keep the action-angle form of the corresponding variables in the transformed Hamiltonian. In this way, we avoid the need to introduce expansions in cartesian variables for this degree of freedom. A general Hamiltonian of this form is

$$H(\phi, I, \xi, \eta) = \omega I + \nu\xi\eta + H_1(\phi, I, \xi, \eta) \quad (15)$$

where i) ν is a real constant, ii) H_1 is periodic in ϕ , and admits a convergent polynomial expansion in the variables (ξ, η) , and iii) H_1 is analytic in a complexified domain $I \in \mathbb{C}$, $|I| < \rho$, $|Im(\phi)| < \sigma$, for two positive constants (ρ, σ) . Similar results apply in models with more than one elliptic degrees of freedom (as, for example, the ‘bicircular’ model of astrodynamics, see Gómez et al. 2001).

Close to the main unstable periodic orbit of the Hamiltonian (12), we look for a transformation from old to new canonical variables $\Phi : (\xi, \phi, \eta, I) \rightarrow (\xi', \phi', \eta', I')$, of the form

$$\begin{aligned} \xi &= \Phi_\xi(\xi', \phi', \eta', I') \\ \phi &= \Phi_\phi(\xi', \phi', \eta', I') \\ \eta &= \Phi_\eta(\xi', \phi', \eta', I') \\ I &= \Phi_I(\xi', \phi', \eta', I') \end{aligned} \quad (16)$$

so that the Hamiltonian in the new variables takes the form:

$$Z_h = \omega I' + \nu\xi'\eta' + Z(I', \xi'\eta') \quad (17)$$

In a Hamiltonian like (17), the quantities I' and $c = \xi'\eta'$ are integrals of motion. Furthermore, for any value of I' , the point $\xi' = \eta' = 0$ corresponds to a periodic orbit, since, from Hamilton’s equations we find $\dot{\xi}' = \dot{\eta}' = 0$, while $\dot{\phi}' = \phi'_0 + (\omega + \partial Z(I', 0)/\partial I')t$. This implies a periodic orbit, with frequency $\omega' = (\omega + \partial Z(I', 0)/\partial I')$. Note that in a system like (12), where the action I is dummy, I' appears in the hyperbolic normal form only through the term $\omega I'$. Thus, in this case the periodic solution $\xi' = \eta' = 0$ has a frequency always equal to ω .

By linearizing Hamilton’s equations of motion near this solution, we find that it is always unstable. In fact, we can easily show that the linearized equations of motion for small variations $\delta\xi', \delta\eta'$ around $\xi' = 0, \eta' = 0$ are

$$\dot{\delta\xi'} = (\nu + \nu_1(I'))\delta\xi', \quad \dot{\delta\eta'} = -(\nu + \nu_1(I'))\delta\eta'$$

where $\nu_1(I') = \partial Z(I', \xi'\eta' = 0)/\partial(\xi'\eta')$. The solutions are $\delta\xi'(t) = \delta\xi'_0 e^{(\nu+\nu_1)t}$, $\delta\eta'(t) = \delta\eta'_0 e^{-(\nu+\nu_1)t}$. After one period $T = 2\pi/\omega$ we have $\delta\xi'(T) = \Lambda_1 \delta\xi'_0$, $\delta\eta'(T) = \Lambda_2 \delta\eta'_0$, where $\Lambda_{1,2} = e^{\pm 2\pi(\nu+\nu_1)/\omega}$. Thus, the two eigendirections of the linearized flow correspond to setting $\delta\xi'_0 = 0$, or $\delta\eta'_0 = 0$, i.e. they coincide with the axes $\xi' = 0$, or $\eta' = 0$. These axes are invariant

under the flow of (17) and, therefore, they constitute the unstable and stable manifolds of the associated periodic orbit P in the new variables ξ', η' .

If we specify the form of the transformation (16), we can pass from the variables (ξ', η') to the variables (ξ, η) , thus finding the form of the invariant manifolds in the original canonical variables as well.

In order to specify the transformation (16), we perform a step by step normalization procedure, using a computer-algebraic program to perform expansions up to a high order. To this end, we split the original Hamiltonian (15) in terms of different orders of smallness, by introducing an artificial parameter λ , called the ‘book-keeping’ parameter, with numerical value equal to $\lambda = 1$ (see Efthymiopoulos 2012a). To every term in the Hamiltonian expansion we then introduce a factor of the form λ^r , indicating that the term is of r -th order of smallness. The book-keeping rule is the following: all monomial terms in the Hamiltonian containing a product of the form $\xi^{s_1} \eta^{s_2}$ acquire a book-keeping factor $\lambda^{s_1+s_2-2}$. After this, we multiply by one more factor λ all the terms multiplied by ϵ .

ii) *Hamiltonian normalization.* The Hamiltonian normalization is accomplished by means of Lie series (see Giorgilli 2001, or Efthymiopoulos 2012a) via the following recursive algorithm: after r consecutive transformations, we pass to new canonical variables $(\xi, \phi, \eta, I) \rightarrow (\xi^{(1)}, \phi^{(1)}, \eta^{(1)}, I^{(1)}) \rightarrow \dots \rightarrow (\xi^{(r)}, \phi^{(r)}, \eta^{(r)}, I^{(r)})$, in which the Hamiltonian has the form:

$$H^{(r)} = Z_0 + \lambda Z_1 + \dots + \lambda^r Z_r + \lambda^{r+1} H_{r+1}^{(r)} + \lambda^{r+2} H_{r+2}^{(r)} + \dots \quad (18)$$

where $Z_0 = \omega I^{(r)} + \nu \xi^{(r)} \eta^{(r)}$. The Hamiltonian term $H_{r+1}^{(r)}$ contains a sum of terms that are not in normal form, denoted by $h_{r+1}^{(r)}$. The $(r+1)$ -th order Lie generating function χ_{r+1} is the solution of the homological equation

$$\{Z_0, \chi_{r+1}\} + \lambda^{r+1} h_{r+1}^{(r)} = 0 \quad (19)$$

where $\{\cdot, \cdot\}$ denotes the Poisson bracket operator. We then compute the new transformed Hamiltonian via

$$H^{(r+1)} = \exp(L_{\chi_{r+1}}) H^{(r)} \quad (20)$$

where $L_\chi = \{\cdot, \chi\}$. This is in normal form up to terms of order $r+1$, namely:

$$H^{(r+1)} = Z_0 + \lambda Z_1 + \dots + \lambda^r Z_r + \lambda^{r+1} Z_{r+1} + \lambda^{r+2} H_{r+2}^{(r+1)} + \dots \quad (21)$$

where $Z_{r+1} = H_{r+1}^{(r)} - h_{r+1}^{(r)}$.

The solution of the homological equation is found by noting that the action of the operator $\{Z_0, \cdot\} = \{\omega I + \nu \xi \eta, \cdot\}$ on monomials of the form $\xi^{s_1} \eta^{s_2} a(I) e^{ik_2 \phi}$ yields

$$\left\{ \omega I + \nu \xi \eta, \xi^{s_1} \eta^{s_2} a(I) e^{ik_2 \phi} \right\} = -[(s_1 - s_2)\nu + i\omega k_2] \xi^{s_1} \eta^{s_2} a(I) e^{ik_2 \phi} .$$

We write $h_{r+1}^{(r)}$ as

$$h_{r+1}^{(r)} = \sum_{(s_1, s_2, k_2) \notin \mathcal{M}} b_{s_1, s_2, k_2}(I) \xi^{s_1} \eta^{s_2} e^{ik_2 \phi}$$

where we omit, for simplicity, superscripts from the notation of all canonical variables, and we set \mathcal{M} as the set:

$$\mathcal{M} = \{(s_1, s_2, k_2) : s_1 = s_2 \text{ and } k_2 = 0\} . \quad (22)$$

Then

$$\chi_{r+1} = \sum_{(s_1, s_2, k_2) \notin \mathcal{M}} \frac{b_{s_1, s_2, k_2}(I)}{(s_1 - s_2)\nu + i\omega k_2} \xi^{s_1} \eta^{s_2} e^{ik_2 \phi} . \quad (23)$$

After computing χ_{r+1} , we compute the next normalized Hamiltonian $H^{(r+1)}$ via Eq.(20). We truncate all expressions up to a given maximum order r_{max} . This completes one step of the normalization algorithm.

Setting the maximum normalization order equal to the truncation order r_{max} , we approximate the new canonical variables corresponding to the final computed normal form as

$$(\phi', \xi', \eta', I') \simeq (\xi^{(r_{max})}, \phi^{(r_{max})}, \eta^{(r_{max})}, I^{(r_{max})}) \quad .$$

The transformation (16) is then approximated by the truncated form of the Lie series composition:

$$\begin{aligned} \xi &= \exp(L_{\chi_{r_{max}}}) \exp(L_{\chi_{r_{max}-1}}) \dots \exp(L_{\chi_1}) \xi^{(r_{max})} \\ \phi &= \exp(L_{\chi_{r_{max}}}) \exp(L_{\chi_{r_{max}-1}}) \dots \exp(L_{\chi_1}) \phi^{(r_{max})} \\ \eta &= \exp(L_{\chi_{r_{max}}}) \exp(L_{\chi_{r_{max}-1}}) \dots \exp(L_{\chi_1}) \eta^{(r_{max})} \\ I &= \exp(L_{\chi_{r_{max}}}) \exp(L_{\chi_{r_{max}-1}}) \dots \exp(L_{\chi_1}) I^{(r_{max})} \quad . \end{aligned} \tag{24}$$

The computation of the transformation (24) completes the implementation of the hyperbolic normal form algorithm. In the computer implementation, the steps are: i) We compute the form of all generating functions $\chi_1, \dots, \chi_{r_{max}}$ as well as the form of the final transformed Hamiltonian $H^{(r_{max})}$. ii) We compute the canonical transformation (24). In the particular case of the Hamiltonian (12), since the action I is a dummy variable, we have the simplifying properties that a) $\phi = \phi^{(r)}$ for all $r > 0$, and b) the dummy action $I^{(r)}$ does not appear in the transformation equations for the variables ξ and η . iii) We identify $\xi^{(r_{max})}, \eta^{(r_{max})}$ as the best possible approximants to the ‘new’ canonical variables ξ', η' . Then, for computing various structures, we assign values to η' and to ξ' , for fixed values of ϕ' . We then compute the values of the original variables (ξ, η) by the transformation (16), and hence, through Eq.(14) the values of p and $\psi = \pi + u$.

3.3 Position of the main unstable periodic orbit

A property of the transformations (24) is that, setting $\xi' = \eta' = 0$ allows for a computation of the whole form of the unstable periodic orbit corresponding to the origin, in the new variables, for various values of the (constant) action I' . This is because in the new variables, for initial conditions $I'(0) = I_0$, $\phi'(0) = \phi_0$ and $\xi'(0) = \eta'(0) = 0$, the normal form (17) implies the trivial evolution $\xi'(t) = \eta'(t) = 0$, and $I'(t) = I_0$, $\phi'(t) = \phi_0 + (\omega + \partial Z(I', 0)/\partial I'|_{I'=I_0}) t$. Substituting these expressions into (16), we compute the functional form of the time evolution of all quantities $\phi(t)$, $I(t)$, and $\xi(t), \eta(t)$ for the periodic orbit expressed in the original variables as well. Finally, using the linear transformation (14) we obtain the same form in the variables $p(t)$ and $\psi(t)$. We note that in this way we can obtain the analytic representation of the periodic orbit in Fourier series depending periodically on the time without using Lindstedt series (cf. Belló et al. 2010).

For the Hamiltonian (12), up to terms of second degree in the book-keeping parameter λ , we find the following formula for the periodic orbit P:

$$\begin{aligned} \psi_P(t) &= \pi + 0.0740741\epsilon \sin t - 0.000726216\epsilon^2 \sin(2t) + \dots \\ p_P(t) &= -0.00592593\epsilon \cos t - 0.00145243\epsilon^2 \cos(2t) + \dots \end{aligned} \tag{25}$$

We note that both functions $\psi_P(t)$ and $p_P(t)$ do not depend on the action I' . As explained above, this is a feature of the specific model considered.

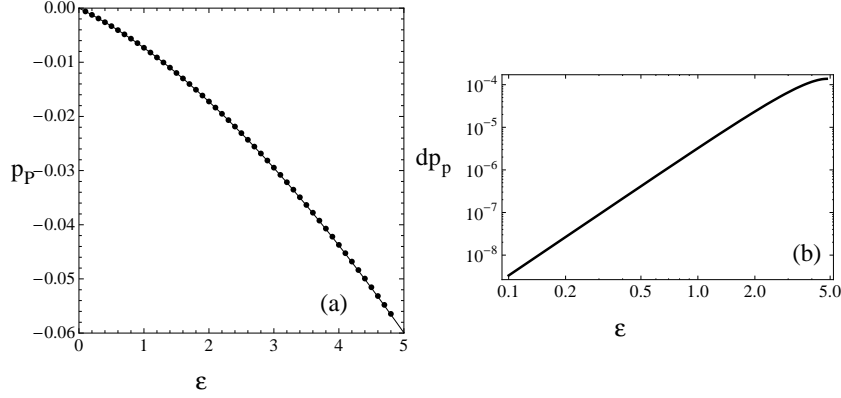


Figure 4: (a) The characteristic curve (position of the initial condition p_P (for $\psi_0 = \phi_0 = 0$) of the main unstable periodic orbit P for the Hamiltonian system (12) as a function of the perturbation parameter ϵ , found analytically (solid line) and by a Newton-Raphson numerical method (points). (b) Difference between numerical and analytical solution at the truncation order $r = 15$.

Setting $t = 0$ in Eqs.(25), we obtain the position of the periodic orbit on the surface of section as a function of ϵ . Figure 4a shows the so-called *characteristic curve* of P. In our case, since we always have $\psi_P = 0$, the characteristic curve simply consists of plotting the initial condition of the periodic orbit $p_P(0)$ on the surface of section versus ϵ . The dotted curve shows $p_P(0)$ as a function of ϵ , computed by a purely numerical process, i.e., implementing Newton's root-finding method, while the solid curve yields $p_P(\epsilon)$ as computed by a hyperbolic normal form at the normalization order $r = 15$. Figure 4b shows the absolute difference between the numerical and the analytical determination as function of ϵ . For fixed $r = 15$, the error is about 3×10^{-9} for $\epsilon = 0.1$ and rises up to 10^{-4} for the highest considered value $\epsilon = 5$. However, since the domain of convergence of the hyperbolic normal form includes always the origin, the computation of the characteristic curve, as well as of the whole form of the periodic orbits, can be made with arbitrarily high precision for all values of ϵ for which we have convergence, by increasing the order of r . Thus, by raising r to about $r = 50$ we are able to recover eight significant digits for values of ϵ as high as $\epsilon = 5$, despite the fact that the motions in the neighborhood of the periodic orbit are very chaotic for such a high value of ϵ .

3.4 Analytical invariant manifolds. Domain of convergence

The unstable manifolds emanating from P in the case of the Hamiltonian model (12) are computed by setting $\eta' = 0$ in the transformation (16). The manifolds are two dimensional, and they are given parametrically by various values of ξ' for a fixed value of the angle ϕ' . Setting $\phi' = 0$ yields the asymptotic curves, i.e., the one-dimensional intersections of the manifolds with the stroboscopic surface of section.

Our first computation refers to the integrable case $\epsilon = 0$. Then, the Hamiltonian (12) becomes simply the pendulum Hamiltonian, and the unstable and stable manifolds simply coincide with the pendulum separatrix. Furthermore, since we are only left with terms containing one couple of canonical variables (ξ, η) , we are able to perform high order, and high precision, computations using Mathematica.

Figure 5a shows the comparison between the exact separatrix and an analytical compu-

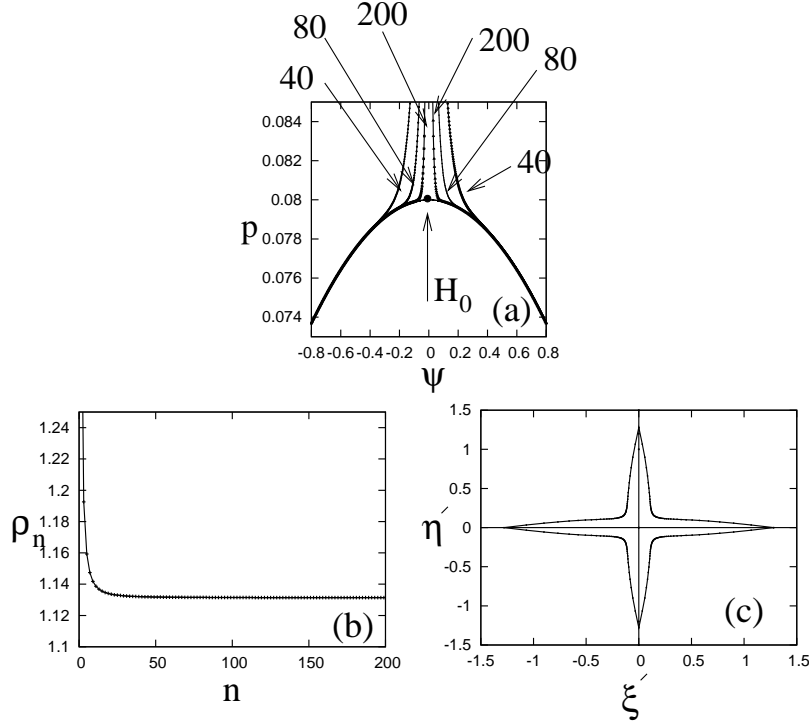


Figure 5: (a) A focus on the uppermost part of the separatrix of the pendulum model (Eq.(12) for $\epsilon = 0$), showing the exact separatrix (thin curve) superposed by the analytical computation of the unstable manifolds (left curves, deviating upwards) and of the stable manifolds (right curves, deviating upwards) at the normalization orders $r = 40$, $r = 80$, and 200 . As r increases, the analytical curves approach closer and closer to the point in the middle of the separatrix, where $\psi = 0$. (b) The D'Alembert sequence ρ_n for the normalizing transformation, setting $\eta = 0$ (see text). In this case, the radius of absolute convergence turns to be finite, as ρ_n stabilizes to $\rho_n = 0.1392$ for larger n . (c) Numerical estimation of the boundary of the domain of convergence around the origin, using the values of the D'Alembert radii computed in different directions on the plane $(\xi'\eta')$.

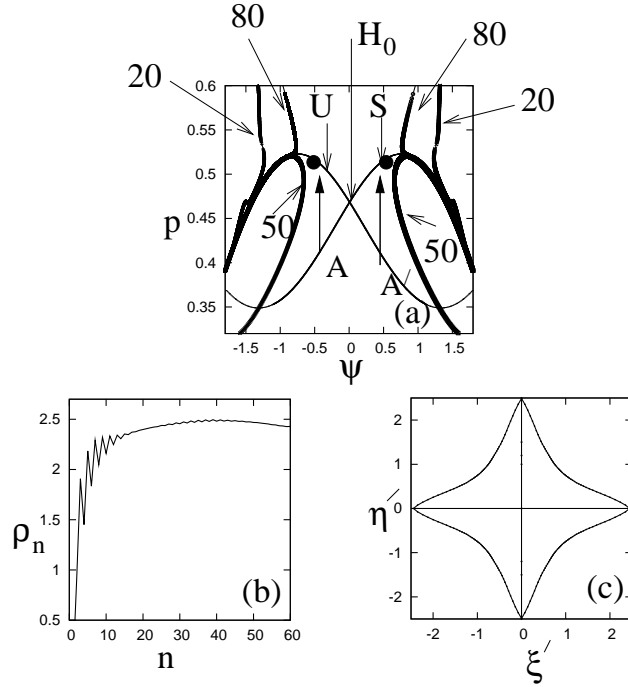


Figure 6: (a) Same as in Fig.5a, but for the asymptotic manifolds of P when $\epsilon = 1$. The analytical manifolds are computed at orders $r = 20$ (deviating upwards), $r = 50$ (deviating downwards), and $r = 80$ (deviating upwards). We observe that no important improvement exists between the orders 50 and 80. A and A' are the limits of convergence of the series along the unstable (U) and stable (S) manifolds. (b) The sequence of d'Alembert radii also indicates a finite radius of absolute convergence along the manifolds at $\rho \sim 2.4$. (c) The domain of absolute convergence, found as in Fig.5c.

tation of the asymptotic manifolds using the hyperbolic normal form at different truncation orders of the normalizing transformation Φ , namely a) $r_{max} = 40$, b) $r_{max} = 80$, and c) $r_{max} = 200$, for $\omega_0 = 0.2\sqrt{2} = 0.2828$. We observe immediately the main effect, namely that the analytical manifolds, even after a truncation order as high as 200, deviate from the separatrix a little before the point $H_0 \equiv (u = \pi, p = 2\omega_0)$. For $\epsilon = 0$ this is the point where the upper branch of the unstable manifold joins smoothly with the upper branch of the stable manifold of P , while, as we will see, for arbitrarily small ϵ , the point H_0 corresponds to a homoclinic intersection of the two manifolds, which takes place always at the angle $u = \pi$ (corresponding to $\psi = 0$).

The fact that we use an 80-digit precision is necessary in order to check the accuracy of our computations. In fact, using the usual 16-digit precision, we find that the accumulation of round-offs in the calculation of the hyperbolic normal form coefficients results in a number of coefficients being affected up to their first digit after the truncation order $r = 56$.

The deviation of the analytical manifolds from the true separatrix shown in Fig.5a is a phenomenon observed also in Vieira and Ozorio de Almeida (1996; their Fig.4). In fact, these authors' computation also points towards the fact that the deviation occurs at a point at which, when the truncation order tends to infinity, the analytical stable and unstable manifolds should join each other smoothly. Here we establish this fact more definitely by using higher order approximations and a much larger number of digits in the calculations.

The above calculation indicates that in the case $\epsilon = 0$ the domain of convergence of the normalizing transformation Φ along the ξ' (and η') axis is finite. However, we can provide a further indication by examining the domain of *absolute* convergence, using, again, the D'Alembert sequence of radii ρ_n , where, in the series yielding the transformation Φ , we set the book-keeping constant equal to $\lambda = 1$ and we rearrange all terms according to the polynomial orders $n = 1, 2, \dots$ in the variables (ξ, η) . The evolution of the sequence ρ_n with n is shown in Fig.5b. We now see that, contrary to the mapping case, in the present case the D'Alembert sequence stabilizes at a finite constant value. Up to the order $n = 200$, we find that variations of the value of ρ_n occur only in the fifth digit and beyond. Thus, we estimate the D'Alembert radius as $\rho = 1.1392\dots$. We can also obtain an estimate of the domain of absolute convergence not only along the axes ξ' or η' , but also along any line of the form $\eta' = \tan(\theta)\xi'$ passing from the origin, for various angles θ . In this case, setting $\xi' = s \cos \theta$, $\eta' = s \sin \theta$, the transformation (16) for the variable, say, ξ , for $\phi' = 0$, leads to

$$\xi = g_1(\theta)''s + g_2(\theta)''s^2 + \dots \quad (26)$$

where s is a length parameter along the chosen line. Thus, implementing Eq.(9), but for the coefficients g_i'' which depend on θ , we can estimate the D'Alembert radius $\rho(\theta)$ in the particular direction. We have checked that the D'Alembert radii ρ_n along all directions have stabilized up to several significant digits at the order $n = 200$. We then use the value ρ_{200} as an estimate of the asymptotic value ρ . Figure 5c shows the result, by computing $\rho(\theta)$ for 360 values of θ from 1 to 360 degrees. Plotting the points $(\xi', \eta') = (\rho \cos \theta, \rho \sin \theta)$, we find the form of the boundary of the domain of absolute convergence. This has a star-like structure, and we see that it is finite for all angles θ .

The fact that the absolute convergence of the hyperbolic normal form series takes place in a finite domain in the particular case of one degree of freedom systems like the pendulum was proven by Johnson and Tucker (2011) using majorant series (see also their figure 2). Since such systems have no chaos, it must be stressed that the finite extent of the domain of convergence is a property of the series and it is not related to chaos.

Passing now to the case $\epsilon = 1$, Figure 6a shows a computation of the invariant manifolds as above, but for the truncation orders $r = 20$, $r = 50$, and $r = 80$. In this case, the number of terms in the corresponding series is so large that it makes higher order calculations quite difficult at precisions higher than the usual double precision level. In fact, we used a fortran program in order to extend the computation to the 80-th order using double precision. However, the accumulation of round-off errors in the series terms results in a loss of accuracy for some coefficients even at the first significant digit after an order $r \sim 40$. This we were able to check by computing the numerical differences between coefficients for which it is known that, by the symmetry of the Hamiltonian (12) with respect to the axis $\psi = 0$, their values should be equal.

Returning to Fig.6a, the qualitative form of the analytical manifolds is quite similar to the corresponding form in the separatrix case (Fig.5a). Namely, the analytical manifolds clearly deviate from the true ones before reaching the position of the homoclinic point H_0 . This indicates that the domain of convergence of the normalizing transformation along the axes ξ' and η' is finite in this case as well. In fact, a simple argument can show that the domain of absolute convergence, for ϵ small, is close to the corresponding domain for $\epsilon = 0$, for all directions θ . This is because we can readily see that the corresponding series for, say, the variable ξ , introduce only $O(\epsilon)$ corrections with respect to the series (26), namely the new series are of the form

$$\xi = h_0(\theta) + (g_1(\theta)'' + h_1(\theta))s + (g_2(\theta)'' + h_2(\theta))s^2 + \dots \quad (27)$$

where all coefficients h_i are of order ϵ . Then, it is trivial to prove that for ϵ sufficiently small the D'Alembert sequence converges to a value $\rho + O(\epsilon)$, where ρ is the convergence radius of the original sequence. As shown in Fig.6b, for $\epsilon = 1$ the sequence ρ_r exhibits a clear tendency to convergence, although with larger fluctuations up to the order 40 than the corresponding sequence of the $\epsilon = 0$ case (Fig.5b). In this case, since the sequence ρ_n seems to stabilize tending asymptotically from above to a constant value, we used a somewhat smaller value than ρ_{40} , namely $\rho = 0.95\rho_{40}$, as an estimate of the radius of absolute convergence.

For $\theta = 0$, we find the value $\xi' = \rho = 2.4$, which represents the radius of convergence in the direction along the unstable manifolds. In the next section, we will present an extended method that allows to parameterize the invariant manifolds at radii beyond ρ . Using that method, we find that the value $\xi' = \rho = 2.4$ corresponds to the point A along the invariant manifolds in Fig.6a, given by $(\psi_A, p_{\psi,A}) = (-0.6146, 0.5208)$. We observe that the analytic computation of the invariant manifolds starts deviating from the numerical one a little before the point A. This verifies the fact that the homoclinic point H_0 is outside the domain of convergence. In fact, computing the hyperbolic series for different values of ϵ yields that the distance of A from H_0 increases as ϵ increases.

Returning to the computation of $\rho(\theta)$, Fig.6c shows the corresponding plot for various angles θ from 0° to 360° . This is qualitatively similar to Fig.(5c), indicating that no important differences regarding the convergence of the hyperbolic normal form exist between the cases $\epsilon = 0$ and $\epsilon = 1$.

In conclusion, our numerical results indicate that, contrary to the case of simple 2D mappings analytic over the whole plane, in the Hamiltonian case the domain of convergence of the hyperbolic normal form has a *finite* extent along the invariant manifolds represented by the axes $\xi' = 0$ and $\eta' = 0$, even if the original Hamiltonian is analytic over its entire phase space. This appears at first to pose a severe limit to the usefulness of the hyperbolic normal forms in this case. In fact, although the calculations of Vieira and Ozorio de Almeida (1996) seemed to indicate that it was possible to compute homoclinic orbits using only the hyperbolic normal form series, a careful inspection of their computations shows that the accurate location of the homoclinic orbits was only possible by using the so-called (by them) 'z-propagation', which means numerical propagation of initial conditions obtained in a small domain around the origin. Thus, this computation was not based exclusively on the use of series.

On the other hand, Ozorio de Almeida and Vieira (1997) discussed also from a theoretical point of view the issue of the extension of Moser's domain of convergence in the Hamiltonian case. Their main argument uses the concept of analytic continuation which allows to represent the flow in time of some initial condition using a series polynomial in the canonical variables. In the following section we will show that in the case of Hamiltonian expressed in power series there are limits to the domain of convergence. This explains the difference between simple mappings and Hamiltonian systems. However, by modifying the method of Ozorio de Almeida and Vieira (1997), we will provide an extended method allowing the computation of the invariant manifolds over a large extent in Hamiltonian models using only series.

4 Extended method

Consider a Hamiltonian function $H(\psi, \phi, p, I)$ periodic in ψ, ϕ , and denote by $q \equiv (\psi, \phi, p, I)$ a set of initial conditions and by $q_t \equiv (\psi_t, \phi_t, p_t, I_t)$ their image at a fixed time t under the flow of H . Fixing t we will consider the domain of analyticity of the mapping in time of the phase-space variables, i.e. the mapping $q_t = F_t(q)$. To this end, we express first $F_t(q)$ via its

Lie series expansion

$$q_t = \exp(L_{tH})q \quad (28)$$

For all variables $(\psi_t, \phi_t, p_t, I_t)$ this takes the form of a Fourier series. For example, we have

$$p_t = \exp(L_{tH})p = \sum_{k_1, k_2} \tilde{f}_{p, (k_1, k_2)}(p, I, t) e^{i(k_1 \psi + k_2 \phi)} \quad (29)$$

with $\tilde{f}_{p, (k_1, k_2)}(p, I, 0)$ equal to p , for $k_1 = k_2 = 0$, and zero otherwise (since the series (29) is a near identity transformation). The Fourier coefficients $\tilde{f}_{p, (k_1, k_2)}(p, I, t)$ are power series of the time variable, i.e. we have

$$\tilde{f}_{p, (k_1, k_2)}(p, I, t) = \tilde{f}_{p, (k_1, k_2)}^{(0)}(p, I) + t \tilde{f}_{p, (k_1, k_2)}^{(1)}(p, I) + t^2 \tilde{f}_{p, (k_1, k_2)}^{(2)}(p, I) + \dots \quad (30)$$

For a fixed value of t , the domain of analyticity of (29) intersects the action space at all points (p, I) for which:

- i) The Taylor series (30) is convergent, and
- ii) There are positive constants $A(p, I), \sigma(p, I)$ such that for all k_1, k_2 we have

$$|\tilde{f}_{p, (k_1, k_2)}(p, I, t)| < A e^{-(|k_1| + |k_2|)\sigma}.$$

The last condition stems from the requirement that the Fourier coefficients $\tilde{f}_{p, (k_1, k_2)}(p, I, t)$ decay exponentially (see Giorgilli 2001, pp.88-90).

In a similar way we can determine the domains of analyticity of the Lie mappings of the form (29) for all other variables. The final domain of analyticity of the mapping F_t is given by the common intersection of all partial domains. Let us denote this domain by D_t .

Assuming that the Hamiltonian H is polynomial in the action variables (p, I) , a key remark is now the following. For fixed (p, I) , regarding the angles the Fourier series (29) are analytic in complex strips of the form $0 \leq \text{Re}(\psi) < 2\pi$, $|\text{Im}(\psi)| < \sigma(p, I)$. This implies that if we Taylor-expand (29) with respect to the angle ψ corresponding to the *hyperbolic degree of freedom* (cf. section 3, Eq.(13)) around some value $\psi_0 \in \mathbb{T}$, the expansion converges only in the interval $|\psi - \psi_0| < \sigma$. Therefore, the polynomial expansion of the mapping F_t in the angular variable corresponding to the hyperbolic degree of freedom converges only in a domain \mathcal{D}_t which is a restriction of D_t , defined by the above inequality.

We may finally consider the composition

$$F_{T, S_T} = F_{t_n} \circ F_{t_{n-1}} \circ \dots \circ F_{t_1}, \quad S_T = \left\{ t_1, t_2, \dots, t_n : \sum_{i=1}^n t_i = T \right\} \quad (31)$$

which maps the variables q to their values q_T at the time $t = T$ (the period of the stroboscopic Poincaré section) through n intermediate mappings at the times $t_1, t_1 + t_2, \dots, t_1 + \dots + t_n = T$. The domain of analyticity D_{T, S_T} of the mapping F_{T, S_T} is a restriction of the domains of analyticity of the mappings F_{t_i} , and its polynomial expansion in the angle corresponding to the hyperbolic degree of freedom converges in a restriction \mathcal{D}_{T, S_T} of the domains \mathcal{D}_{t_i} .

We denote now by Δ_T the union of the sets \mathcal{D}_{T, S_T} for all possible choices of S_T such that the sets \mathcal{D}_{T, S_T} include the unstable periodic orbit P . Then, according to Da Silva Ritter et al. (1987), the normalizing transformation Φ of the hyperbolic normal form around P is convergent in a domain of the new canonical variables (ψ', ϕ', p', I') whose image is the set

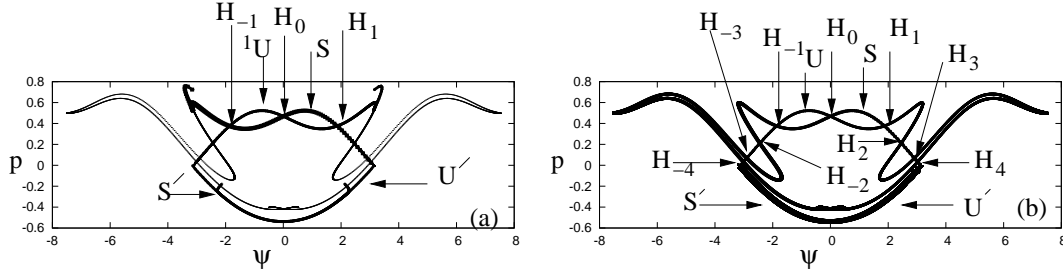


Figure 7: Analytical invariant manifolds for $\epsilon = 1$ computed with the extended method setting (a) $m = 1$ and (b) $m = 3$. In the first case, the analytical manifolds intersect at the first and second homoclinic points H_0 , H_1 (or H_{-1}), and deviate afterwards. The position of these points can be computed with high accuracy using only series. In the second case, the analytical manifolds reproduce many features of the homoclinic tangle, including the oscillations of at least third order lobes.

Δ_T . Following the argument of Ozorio de Almeida and Vieira (1997), we have then the result that the domain of convergence of the hyperbolic normal form can be extended, from the original Moser's domain, all over the domain Δ_T . However, as we have seen in the previous section, the numerical indications are that the domain Δ_T contains no homoclinic points. Thus, with the usual polynomial series expansion for the angle ψ we cannot go beyond such homoclinic points.

If, however, we maintain the Fourier form of the transformations like (29), without expanding the trigonometric terms with respect to the angle ψ , then we can obtain a computation of the invariant manifolds in a domain beyond Δ_T . To this end, we define the set of extended transformations:

$$\Phi_m = F_T^m \circ \Phi \circ N_T^{-m}, \quad m = 0, \pm 1, \pm 2, \dots \quad (32)$$

where

i) N_T is the mapping of the new canonical variables (ξ', η') after m periods under the normal form (17). This is trivially found by the normal form equations of motion (see section 3).

ii) we analyze F_T as a composition of the form (31), keeping each of the functions F_{t_i} in its original form, given by a Fourier series of the form (29).

In words, Eq.(32) means the following procedure, which uses only series computations: starting from a point (ψ', ϕ', p', I') in the new variables, i) compute its m -th pre-image (or image, for $m < 0$) with period T under the normal form series dynamics, ii) use the transformation series Φ to compute the values of the old canonical variables corresponding to the last point found in step (i), and finally iii) use the truncated Fourier series F_T^m in order to map forward (or backward, for $m < 0$) for m periods the point found in (ii).

In the numerical examples given below, we choose S_T as $S_T = \{T/4, T/4, T/4, T/4\}$. Other choices of the separation of T in a small number of parts are possible, but we found that the choice $S_T = \{T/4, T/4, T/4, T/4\}$ is simple and works with good precision for all initial conditions in the whole domain where the asymptotic invariant manifolds extend. Thus, by this choice we are able to compute the asymptotic invariant manifolds over a large length using only series (a preliminary computation of this type was done in Efthymiopoulos (2012b)).

As an example, Figure 7 shows a computation of the asymptotic manifolds when $\epsilon = 1$, and m in the extended transformation (32) is chosen as $m = 1$ (Fig.7a), or $m = 3$ (Fig.7b) for the unstable manifolds, and $m = -1$, $m = -3$ for the stable manifolds. We now see that the analytical computation in the second case is able to yield the homoclinic points $H, H_1, H_{-1}, H_2, H_{-2}, \dots$, corresponding to the intersections of the upper branches of the invariant manifolds. In the same way, we can locate the homoclinic intersections of the lower branches of the manifolds. The latter, however, develop oscillations of a very small extent, while the upper manifolds develop lobes defined by oscillations, back and forth, over a scale about three times as large as the whole extent of the separatrix of the unperturbed case.

Since in practice the extended mappings (32) are computed by finite truncations of the Lie series for the mapping N_T^{-m} as well as the normalizing transformation Φ , the accuracy of the extended method depends only on the order of truncation. We check the accuracy of N_T by computing how well the energy is preserved in the mapping, under N_T , of initial conditions and their images on the stroboscopic surface of section. As an indication, at the 30th order of truncation the energy is preserved to about six digits close to the neighborhood of the first homoclinic point. This sets the overall precision of the method.

The union of all extended mappings (32) for $m = \pm 1, \pm 2, \dots$ provides the complete parametrization of the unstable or stable manifolds in terms of the ‘length’ parameters ξ' or η' . In practice, however, we can only choose finite values of m . Then, the parametrization can be computed up to a finite maximum value of ξ' (or η'), satisfying the relation $|\xi'|_{max} = \rho \lambda^m$, where $\lambda = e^{\nu T}$, and ρ is the radius of convergence of the initial series of the canonical transformation Φ . In our model example, we find $\lambda = 5.91$, while (from Fig.6b) $\rho \simeq 2.4$. Thus, with m as high as $m = 3$, we find $|\xi|_{max} \simeq 5 \times 10^2$, i.e. the parametrization extends to a length about 200 times larger than the length found by the original Moser normal form series. But if we take m even larger, we can find theoretically the asymptotic curves up to an arbitrarily large extent.

These properties of the extended method have immediate application in locating the homoclinic points and a number of other features of the homoclinic tangle and its neighborhood. In order to compute a homoclinic point, we consider the quantities ξ , along the unstable manifold, and η , along the stable manifold, as parameters whose values can be varied. We then use a root-finding method (like Newton-Raphson) to compute a homoclinic point as follows. Determining, via the extended transformations (32) the transformations $p(\xi, \eta), \psi(\xi, \eta)$, we solve simultaneously the equations

$$K(\xi, \eta) = p(\xi, 0) - p(0, \eta) = 0, \quad L(\xi, \eta) = \psi(\xi, 0) - \psi(0, \eta) = 0 \quad . \quad (33)$$

In the use of Newton-Raphson, all partial derivatives appearing in the extended transformation are given in the form of truncated series, since, by the chain rule, the Jacobian matrix $\partial(K, L)/\partial(\xi, \eta)$ can be computed by the product of the Jacobian matrices of all functions participating in the function composition (32). In particular, expressing the part N_T^{-m} as Lie series is crucial in analytically computing the parametrizations used in the quantities K, L as well as their derivatives. As a result, the accuracy of the present method is only limited by the accuracy of the various truncations in the computed series. For example, we compute the position of the homoclinic point H_0 in Fig.(6a) using the extended transformation (32) for $m = 1$. We have $\psi = 0$, while for p_{H_0} we find $p = 0.5592605371492\dots$ with a precision of 13 significant digits.

Finally, the extended mappings (32) offer the possibility to compute curves in the chaotic domain corresponding to values of c different from zero. Such curves can be ‘invariant’ or ‘quasi-invariant’. Namely, while the hyperbolic normal form converges all along a hyperbola

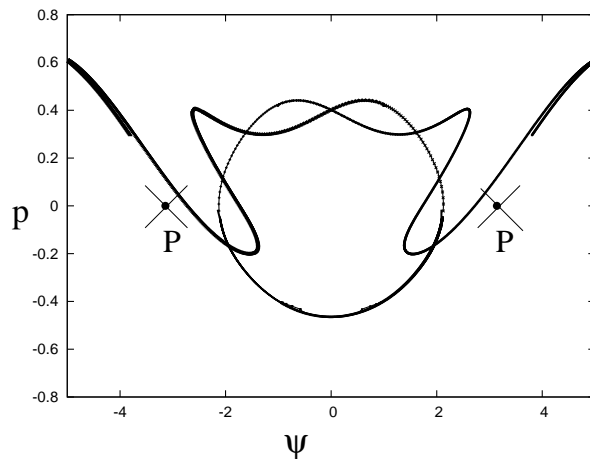


Figure 8: A curve of the form $\xi'\eta' = c$, mapped in the old variables, for $c = -0.15$, computed with the extended transformation $m = 2$. The unstable periodic orbit is represented by the point P.

in the variables ξ', η' defined by $\xi'\eta' = c$, with $c \neq 0$, it is possible that only finite segments of the hyperbola map onto segments of the same hyperbola within the domain of convergence of the normalizing transformation Φ . This implies that, even using the extended transformations 32, one may not be able to define a continuous set that maps exclusively onto itself at successive iterations. On the other hand, for small values of c the curves $\xi'\eta' = c$ are invariant. In practice, it is difficult to find the limiting value of c up to which we obtain such invariant curves.

To our knowledge, the properties of such curves have not so far been studied. Figure 8 shows an example of the form of the curves corresponding to the value $c = \xi'\eta' = -0.15$ in the model (12) (we find that negatives values of c correspond to curves in the interior domain defined by the invariant manifolds up to the homoclinic intersection H_0 , while $c > 0$ corresponds to curves in the exterior domain). In order to compute the curves, we use a unique parameter, say, $s = \xi$, $\eta = c/s$, and make sure that the mapping N_T^m (for m positive or negative) brings the points corresponding to the chosen range of values of s within the domain of convergence of Moser's series for the transformation Φ .

In Fig.8 we observe that the curve of $c = -0.15$ follows in general a path parallel to the paths of the asymptotic manifolds (cf. Fig.7). Furthermore, the curves with $c \neq 0$ have a number of self-intersections. Such intersections define points accumulating to some homoclinic points as $c \rightarrow 0$. However, there are also intersections developed between the curves, that do not accumulate around homoclinic points. In fact, similarly to Da Silva Ritter et al. (1987), we can use the computation of the intersections between one or more curves, for $c \neq 0$, in order to compute high order periodic orbits accumulating to some homoclinic points. The study of such orbits is of particular interest, since they are related to the definition and statistics of the *recurrence times* in the domain of homoclinic chaos (see Contopoulos and Polymilis 1993). Their study using analytical series methods is proposed for future work.

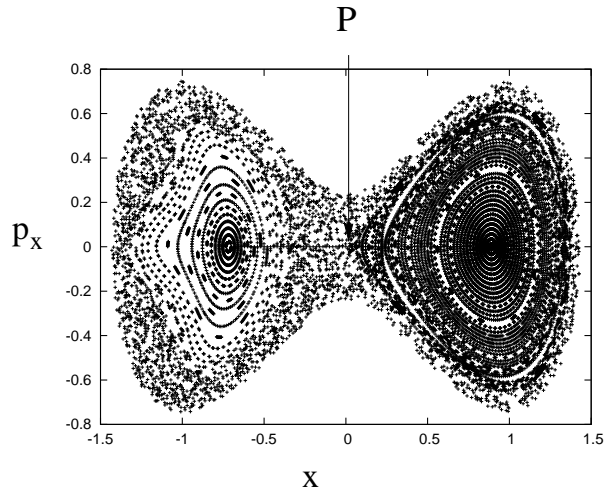


Figure 9: The Poincaré surface of section (x, p_x) , for $y = 0, p_y > 0$, in the Hamiltonian model (34), for the energy $E = H = 0.03$. The main unstable periodic orbit is represented by the point P.

5 Unstable equilibria in a polynomial Hamiltonian model

The example of the Hamiltonian (12) dealt with in sections 3 and 4 represents a time-dependent Hamiltonian system which is reduced to an autonomous two-degrees of freedom system via the use of the action-angle variables (I, ϕ) . Nevertheless, this system differs from the systems considered in the theorems of Moser (1958) and Giorgilli (2001) because, if we introduce the Cartesian canonical variables $x = \sqrt{2I} \sin \phi$, $p_x = \sqrt{2I} \cos \phi$, the Hamiltonian (12) is not polynomial in (x, p_x) . Then, one may wonder whether the results of sections 3 and 4 are applicable in the polynomial case considered by Moser and Giorgilli.

In order to investigate this question, we consider the Hamiltonian model

$$H = \frac{1}{2}(p_x^2 - x^2) + \frac{1}{2}(p_y^2 + y^2) + xy^2 + x^2y^2 + x^4/4 \quad . \quad (34)$$

The Hamiltonian flow of (34) yields an unstable equilibrium at $x = y = p_x = p_y = 0$. The corresponding energy is $E = H = 0$. On the other hand, for $E > 0$ the unstable equilibrium solution is continued as an unstable periodic orbit solution. Figure 9 shows a Poincaré surface of section $y = 0, p_y > 0$ at the energy $E = 0.03$. The periodic orbit (denoted by P) intersects the Poincaré section at $x_P = 0.0246122$, $p_{x,P} = 0$. We observe the formation of a figure-eight type chaotic layer due to the homoclinic chaos around P.

We now implement the algorithm described in subsection 3.2 in order to compute analytically the invariant manifolds emanating from P. In this case, the algorithm becomes equivalent to the algorithm described in Giorgilli (2001) after the substitution $y = (2I)^{1/2} \sin \phi$, $p_y = (2I)^{1/2} \cos \phi$, $x = (\xi - \eta)/\sqrt{2}$, $p_x = (\xi + \eta)/\sqrt{2}$, $\nu = 1$. Finally, we choose our book-keeping to follow the ordering by polynomial degree, i.e., terms of book-keeping order s correspond to terms of degree $s + 2$ in the variables (y, p_y, ξ, η) .

We compute the hyperbolic normal form (Eq.(17)), as well as the corresponding near-identity transformations (Eq.(16)) up to the order $s = 43$. In the new canonical variables (ξ', η', ϕ', I') the first few terms of the normal form read

$$E = Z_h = I' + \xi' \eta' - 0.6 I' \xi' \eta' + 0.55 I'^2 \dots \quad (35)$$

We note that no small parameter (like ϵ in the model of sections 3 and 4) appears in the normal form (35). Here, however, the periodic orbit P, and its associated manifolds, are parameterized by the value of the energy E , or of the action $I' = I_0$ found by setting $\xi' = \eta' = 0$ in Eq.(35) and solving the equation for I' for a given value of E . For $E = 0.03$ we find $I_0 = 0.0295075$. The corresponding period is given by $T_0 = 2\pi/\omega(I_0) = 6.07748$, where $\omega = dZ_h/dI_0$.

In the computation of the invariant manifolds, it is convenient to determine as surface of section one in which all initial conditions on the manifolds return at equal times $t = T_0$. This surface of section corresponds to the choice $\phi' = 0$, for points of the unstable manifold, or $\phi' = \pi$ for points of the stable manifold.

Setting $I' = I_0, \phi' = 0$, we obtain all four canonical variables x, p_x, y, p_y as polynomial series of the two variables ξ', η' . An important consistency check is to replace these series in the Hamiltonian (34). Then, we find that all series coefficients cancel (to a numerical precision 10^{-15} , leaving only a constant equal to 0.03, i.e., the numerical value of the energy corresponding to I_0).

Figure 10a shows, now, the computation of the invariant manifolds of P numerically, as compared with the analytic manifolds produced by the hyperbolic normal form series truncated at the orders 15 and 43. We observe that, as the order of truncation increases, the analytic unstable manifold tends to coincide with the numerical one up to a point that comes closer and closer to the point A in Fig.10a. This point corresponds to an approximation of the domain of convergence of the normal form transformation series, as computed numerically using, again, d'Alembert's criterion. Similarly, the analytic stable manifold, which is symmetric with respect to the unstable one with respect to the axis $p_x = 0$, starts deviating from the numerical one a little before A', i.e. the point symmetric to A.

Figure 10b, now, shows the result of using the extended method of section 4 in the present example. Here, we implemented Cauchy's criterion in order to determine the distance from the origin of the nearest singularity of the Hamiltonian flow in the complex time domain for all initial conditions in the range $-1.5 \leq x \leq 1.5, -1 \leq p_x \leq 1$. We find that all singularities are at distances larger than $|t| = 1$. Thus, we used a partition in eight time steps of length $\Delta t = T_0/8$, to ensure that the extended series converge for all initial conditions considered. We observe that the extended series are able to reproduce the numerical asymptotic curves up to a length covering at least the homoclinic points H_0, H_1, H_2, H_3 , and H_{-1}, H_{-2}, H_{-3} . Furthermore, for the used value of E , the analytical manifolds are also able to reproduce higher order homoclinic intersections developed among some low order lobes of the invariant manifolds, whose size, at this particular energy, is sufficient for them to intersect.

In conclusion, the main conjectures and results found for generic action-angle systems of the form considered in our present formalism appear also in the original case examined by Moser, i.e., of polynomial Hamiltonian systems with unstable equilibria.

6 Conclusions and Discussion

We studied the convergence properties of the hyperbolic normal form series used in the computation of the invariant manifolds of an unstable equilibrium point, or an unstable periodic orbit, in 2D mappings and in 2D generic Hamiltonian systems expressed in action-angle variables. Our main findings can be summarized as follows:

1) In 2D mappings analytic over their whole phase space, we confirmed by numerical experiments the statement of Da Silva Ritter et al. (1987) that the convergence of the normal form extends to infinity along the invariant manifolds, and to finite, but large domain,

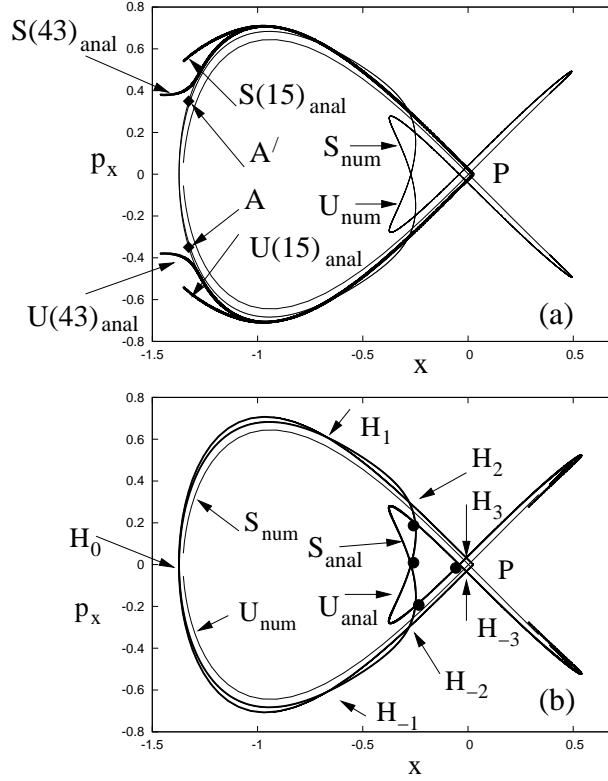


Figure 10: (a) Analytical (thick lines) versus numerical (thin lines) invariant manifolds in the model (34), at the energy $E = 0.03$, in the surface of section given by $\phi' = 0$, for the unstable manifold, or $\phi' = \pi$ for the stable manifold, where ϕ' is the angle in the new variables in the elliptic degree of freedom after implementing the normal form transformations (see text). The analytical manifolds are computed at the truncation orders $r = 15$ and $r = 43$. The points A and A' represent the limit of convergence of the series along the unstable and stable manifolds respectively. (b) Same as in (a), but now with for the analytical manifolds computed by the extended method of section 4. The analytical manifolds now reproduce well several lobes of the numerical ones, and they can be used to locate the position of the homoclinic points H_0 and $H_{\pm j}$, $j = 1, 2, 3$. The thick dots represent higher order homoclinic points reproduced by the same computation.

for nearby ‘quasi-invariant’ curves. This allows in practice for the computation of many interesting features of the homoclinic tangle using only series (e.g. homoclinic points, periodic orbits of high period, high order lobes of the invariant manifolds etc.)

2) In two different 2D mappings that we studied, the rate by which the sequence of D’Alembert radii of the formal series goes to infinity is found to obey different laws. In the standard map it is found to grow logarithmically with the normalization order r , while in the Hénon map it is quadratic in r . However, when back-transforming to the original variables, in both cases the length along the manifolds recovered by the truncated analytical series increases with the truncation order r as $\log(r)$. Finally, if a mapping has a limited analyticity domain, then the sequence of D’Alembert radii tends to a constant, indicating that the domain of convergence in this case is finite.

3) As a first example of the Hamiltonian case, we studied a pendulum model with periodic perturbation, which cannot be reduced to a polynomial form. We find a finite domain of convergence of the hyperbolic normal form, and we provide results indicating that this domain does not reach any homoclinic point. We also give the form of the domain of convergence on the plane of the new hyperbolic canonical variables. Finally, we checked the accuracy of our computations when computing the normal form series using the usual double precision, or 80-digit precision. The latter is needed in order to control the propagation of round-offs in some cases, beyond a high normalization order.

4) Then, we proposed a new method by which one can compute extensions of the original normalizing transformations of Moser using only series. Thus we materialize the idea of analytic continuation proposed by Ozorio de Almeida and Viera (1997). However, contrary to these authors, we choose action angle variables to represent the series yielding a part of the extended transformation (namely the mappings F^m in Eq.(32)), without expanding the trigonometric functions of the angle corresponding to the hyperbolic degree of freedom in power series. In this way, it becomes possible to parameterize the invariant manifolds up to an arbitrarily large extent. We show the efficiency of the method by concrete numerical examples.

5) We emphasized the fact that the possibility to extend the normalizing transformations to a large domain allows one to study features of chaos using only series. In particular, we approximate the intricate lobes formed by the asymptotic manifolds near the unstable point, and we compute curves of the form $c = \xi'\eta'$ (mapped in the old variables), which are near the asymptotic manifolds. We call these features ‘the structure of chaos’. We propose to use the same approach in order to compute high order periodic orbits that accumulate around one or more homoclinic points.

6) We finally study the case of a polynomial Hamiltonian model, in which the original normal form of Moser is applicable. In this case as well we confirm the results of sections 3, and 4, namely i) we provide numerical evidence that the convergence domain of Moser’s normalizing transformations does not reach any homoclinic point, and ii) that an extension using our method of section 4 allows to parameterize the manifolds over an extent long enough to include several homoclinic points.

The results found so far point towards a number of applications and extensions. In particular, we emphasize two benefits from the extended transformations (32): i) the possibility to obtain a parametrization of the invariant manifolds over an arbitrary length, and ii) the possibility, in numerical implementations, to obtain the manifolds with uniform linear sampling density over any desired length, using higher values of the multiplicity m (see Eq.(32)) to achieve the same density for a longer length. Property (i) marks the essential difference between our new method and previous numerical methods that simply propagate forward initial

conditions obtained by accurate calculations within the domain of convergence of the original method of Moser. Property (ii), on the other hand, is useful in practical computations and visualizations of asymptotic orbits, up to an arbitrarily long extent.

On the other hand, the possibility to represent analytically not only the asymptotic manifolds, but also other invariant manifolds in the neighborhood of an unstable orbit poses a number of interesting theoretical questions related to the structure of chaos in such a neighborhood. In particular, it is known (Contopoulos et al. 1996) that tiny islands of stability can exist arbitrarily close to the unstable fixed point. Such islands are found both outside and inside lobes. According to the Newhouse theorem (Newhouse 1977) such islands are generated by new (irregular) periodic orbits which appear near points of tangency between the stable and unstable asymptotic manifolds. In systems with a compact phase space, such points are generated continuously, for arbitrarily high values of the non-linearity parameter (Contopoulos et al. 1994). In fact, the method of analytic computation of the invariant manifolds lends itself to the computation of such points of tangency of an arbitrarily high order. However, the curves $\xi'\eta' = c$ for $c \neq 0$ cannot represent the islands of the stable irregular periodic orbits.

In the model studied in the present paper, the asymptotic invariant manifolds emanating from the periodic orbit at $\psi = -\pi$ can be formally considered as forming heteroclinic intersections with the manifolds emanating from the periodic orbit at $\psi = \pi$. However the second orbit is the same with the first one modulo 2π . On the other hand, the present method can be used with little modification in order to study true heteroclinic connections between more than one periodic orbits. In fact, this is the case in the model studied by Vieira and Ozorio de Almeida (1996), which possesses a triple periodic orbit. Similar results can be found for unstable periodic orbits of any multiplicity.

There are also examples (e.g. Polymilis et al. 2003) in which, after a period doubling bifurcation, the homoclinic connections between some periodic orbit evolve, by varying one parameter, to heteroclinic connections between two different unstable periodic orbits. The transition from homoclinic to heteroclinic dynamics takes place at the point of the period doubling. The study of such connections by analytical invariant manifolds can provide important information on the kinds and statistics of the recurrences, as well as the transport phenomena taking place in the heteroclinic tangle and its neighborhood.

Acknowledgements: This research has been supported in part by the Research Committee of the Academy of Athens (grant 200/815).

References

- [1] Bartlett, J.H.: 1978, Instability of an area-Preserving Polynomial Mapping, *Cel. Mech.* 17, 3.
- [2] Bartlett, J.H.: 1982, Limits of stability for an area-preserving polynomial mapping, *Cel. Mech.* 28, 295.
- [3] Bartlett, J.H.: 1989, Almost stable regions for an area-preserving mapping, *Cel. Mech. Dyn. Astron.*, 46, 129.
- [4] Bazzani, A., Giovannozzi, M., Servizi, G., Todesco, E., and Turchetti, G.: 1993, Resonant normal forms, interpolating Hamiltonians and stability analysis of area preserving maps, *Physica D*, 64, 66.

- [5] Belló, M., Gómez, G., and Masdemont, J.J.: 2010, Invariant Manifolds, Lagrangian Trajectories and Space Mission Design in Perozzi, E., and Ferraz-Mello, S. (eds), Space Manifold Dynamics, Springer.
- [6] Bongini, L., Bazzani, A., and Turchetti, G.: 2001, Analysis of a model for resonant extraction of intense beams by normal forms and frequency map, *Phys. Rev. Sp. Topics*, 4, 114201.
- [7] Bruno, A.D., 1971, *Trans. Moscow Math. Soc.* 25, 131.
- [8] Bruno, A.D., 1989, *Local Methods in Nonlinear Differential Equations*, Springer, Berlin.
- [9] Cabré, X., Fontich, E., and de la Llave, R., 2005, The parameterization method for invariant manifolds III: overview and application, *Jour. Diff. Eq.*, 218, 444.
- [10] Campagnola, S., Sherritt, P., and Russell, R.P., 2012, Flybys in the Planar Circular Restricted Three Body Problem, *Cel. Mech. Dyn. Astron.*, 113, 343.
- [11] Cherry, T.M., 1926, On the solutions of Hamiltonian systems in the neighborhood of a singular point, *Proc. London Math. Soc. Ser.2*, 27, 151-170.
- [12] Contopoulos, G.: 1990, Asymptotic curves and escapes in Hamiltonian systems, *Astron. Astrophys.*, 231, 41.
- [13] Contopoulos, G., and Polymilis, C. 1993, Geometrical and dynamical properties of homoclinic tangles in a simple Hamiltonian system, *Phys. Rev. E*, 47, 1546.
- [14] Contopoulos, G., Papadaki, H., and Polymilis, C. 1994, The structure of chaos in a potential without escapes, *Cel. Mech. Dyn. Astron.* 60, 249.
- [15] Contopoulos, G., Groussouzakou, E., and Polymilis, C. 1996, Distribution of Periodic Orbits and the Homoclinic Tangle, *Cel. Mech. Dyn. Astron.* 64, 363.
- [16] Contopoulos, G. 2002, *Order and Chaos in Dynamical Astronomy*, Springer, Berlin.
- [17] Da Silva Ritter, G.I., Ozorio de Almeida, A.M., & Douady, R., 1987, Analytical determination of unstable periodic orbits in area preserving maps *Physica D*, 29, 181.
- [18] Delshams, A., and Lázaro, J.T., 2005, Pseudo-normal form near saddle-center or saddle-focus equilibria, *J. Differential Equations*, 208, 312.
- [19] Deprit, A., and Henrard, J., 1969, Construction of Orbits Asymptotic to a Periodic Orbit, *Astron. J.*, 74, 308.
- [20] Efthymiopoulos, C., 2012a, Canonical perturbation theory, stability and diffusion in Hamiltonian systems: applications in dynamical astronomy, in P. M. Cincotta, C. M. Giordano and C. Efthymiopoulos (eds), *Third La Plata Internat. School on Astron. Geophys.: Asociación Argentina de Astronomía*.
- [21] Efthymiopoulos, C.: 2012b, Hyperbolic Normal Forms and Invariant Manifolds. *Astronomical Applications*, *Serbian Astr. J.*, 184, 1.
- [22] Evans, T.E., Roeder, R.K.W., Carter, J.A., and Rapoport, B.I., 2004, Homoclinic tangles, bifurcations and edge stochasticity in diverted tokamaks, *Contrib. Plasma Phys.*, 44, 235.

- [23] Franceschini, V., and Russo, L.: 1981, Stable and unstable manifolds of the Henon mapping, *J. Stat. Phys.*, 25, 757.
- [24] Giorgilli, A 2001, Unstable equilibria of Hamiltonian systems, *Disc. Cont. Dyn. Sys.*, 7, 855.
- [25] Giorgilli, A. 2002, Notes on exponential stability of Hamiltonian systems, *Pubblicazioni della Classe di Scienze, Scuola Normale Superiore, Pisa. Centro di Ricerca Matematica "Ennio De Giorgi"*.
- [26] Gómez, G., Jorba, A., Masdemont, J., and Simó, C., 2011, Dynamics and Mission Design near Libration Points, Vol.IV, Advanced Methods for Triangular Points, Ch.3, World Scientific.
- [27] Gómez, G., and Barrabés, E. 2011, Space Manifold dynamics, *Scholarpedia* 6(2), 10597.
- [28] Grover, P., and Ross, S. 2009, Designing Trajectories in a Planet-Moon Environment using the Controlled Keplerian Map, *Journal of Guidance, Control and Dynamics* 32, 436.
- [29] Johnson, T., and Tucker, W., Qual.: 2011, *Theory Dyn. Sys.* 10, 107.
- [30] Jorba, À., and Masdemont, J., 1999, Dynamics in the center manifold of the collinear points of the restricted three body problem, *Physica D*, 132, 189.
- [31] Moser, J 1956, *Commun. Pure Applied Math.*, 9, 673.
- [32] Moser, J 1958, *Commun. Pure Applied Math.*, 11, 257.
- [33] Newhouse, S.E.: 1977, *Am. J. Math.*, 99, 1061.
- [34] Ozorio de Almeida, A.M., and Vieira, W.M. 1997, Extended convergence of normal forms around unstable equilibria, *Phys. Lett. A*, 227, 298.
- [35] Perozzi, E., and Ferraz-Mello, S. 2010, *Space Manifold Dynamics*, Springer.
- [36] Poincaré, H., 1890, *Journal de Mathematiques Pures et Appliquées*, 6, 313.
- [37] Polymilis, C., Contopoulos, G., and Dokoumetzidis, A., 2003, The Homoclinic Tangle of A 1:2 Resonance in a 2-D Hamiltonian System, *Cel. Mech. Dyn. Astron.*, 85, 105.
- [38] Roeder, R.K.W., Rapoport, B.I., and Evans, T.E.: 2003, Explicit calculations of homoclinic tangles in tokamaks, *Phys. Plasmas*, 10, 3796.
- [39] Rom-Kedar, V., 1990, Transport rates of a class of two-dimensional maps and flows, *Physica D*, 43, 229.
- [40] Ross, S.D., and Scheeres, D.J., 2007, Multiple Gravity Assists, Capture and Escape in the Restricted Three Body Problem, *SIAM J. Appl. Dyn. Syst.*, 6(3), 576.
- [41] Simó, C.: 1990, On the Analytical and Numerical Approximation of Invariant Manifolds, in D. Benest and C. Froeschlé (eds), *‘Les Méthodes Modernes de la Macanique Céleste*, Editions Frontieres, Paris.
- [42] Vieira, W.M., and Ozoiro de Almeida, A.M., 1996, Study of chaos in hamiltonian systems via convergent normal forms, *Physica D*, 90, 9.